Energy Science & Engineering

WILEY

ORIGINAL ARTICLE OPEN ACCESS

Hybrid Oxygen Enrichment and Preheating Strategy for Performance Recovery in Ultra-Lean Micro–Trapped Vortex Combustors

Anouar Benzitouni[1] | Abdelhakim Settar[2] | Boudinar Naouam[1] | Salaheddine Azzouz[1] | Zakaria Mansouri[3]

[1]National Higher School of Technology and Engineering, Laboratory of Energy Systems Technologies (LTSE), Annaba, Algeria | [2]INSA Centre Val de Loire, Université Orléans, PRISME EA, Bourges, France | [3]Department of Engineering, Nottingham Trent University, Nottingham, UK

Correspondence: Zakaria Mansouri (zak.mansouri@ntu.ac.uk)

Received: 5 December 2025 | **Revised:** 15 March 2026 | **Accepted:** 19 March 2026

Funding: Algerian Ministry of Higher Education and Scientific Research

Keywords: micro-combustion | numerical simulation | oxygen enrichment | preheating | thermal performance | thermophotovoltaic system

ABSTRACT

Ultra-lean operation in micro-combustion-based thermophotovoltaic systems offers significant benefits including low pollutant emissions and increased longevity due to reduced thermal stresses, but it is hindered by low thermal performance. This paper numerically addresses the potential of oxygen enrichment and preheating to counteract performance losses in a hydrogen-powered micro-trapped vortex combustor operating under ultra-lean conditions. A Taguchi design of 16 cases was conducted at a fixed equivalence ratio of $\phi = 0.3$, varying inlet temperature from 300 to 450 K and O_2 levels from 21% to 30%, to evaluate their impact on radiative power, energy conversion efficiency, combustion efficiency, and NO_x emissions. Results indicate that excessive enrichment (30% O_2) at high inlet temperature (≥ 400 K) leads to flame flashback, establishing an upper safety limit. Within the stable operating region, O_2 enrichment substantially improved radiative power by up to 56%, while preheating enhanced radiative efficiency by up to 73%, with both factors exhibiting equal influence on combustion efficiency. However, the use of oxygen-enriched air remarkably increased NOx emissions compared to the baseline case at 21% O_2. Moreover, the optimal configuration with $T_{in} = 450$ K and $X_{O2} = 0.27$ has achieved 41% higher energy efficiency and 99% lower pollutant emissions compared to the lean case at $\phi = 0.8$.

1 | Introduction

Recent advances in micro-technology and microelectromechanical systems (MEMS) have revolutionized various fields, such as electronics, medicine, and aviation, due to their reduced weight and long lifetime [1], which has resulted in an increase in demand for more robust power generators other than traditional lithium-ion batteries. One viable solution is the Micro-Thermophotovoltaic (MTPV) system, which is based on the direct conversion of thermal energy released by the micro-combustor into electrical energy using PV cells [2, 3]. This system offers higher energy density, a compact design, and the advantage of having no moving parts. As part of the global shift towards renewable energy to mitigate the environmental impact of CO2 emissions, the depletion of fossil fuel resources, and the ensuing energy crisis, the use of zero-carbon fuels such as hydrogen is becoming essential to drive the next generation of MEMS.

Despite their attractive features, MTPV systems still face major challenges that are primarily related to micro-scale effects such as (1) the intensified heat losses due to high area-to-volume ratio that render the flame more susceptible to quenching, (2) the very short residence time that leads to low combustion efficiency, (3) flame blow-off at high flow velocities, and (4) their inability to operate under ultra-lean regime (equivalence ratio $\phi < 0.5$) [4–6]. This latter constraint is very critical

considering the numerous advantages of ultra-lean combustion which comprise: lower NOx emissions, reduced thermal stresses leading to improved material lifetimes, minimized risks of flame flashback, improved safety compared to full-load regime especially when using highly flammable fuels like hydrogen and finally, ultra-lean operation would achieve better fuel economy provided that flame stability and radiative efficiency are maintained therefore enabling robust and efficient performance.

According to literature, a great number of works have been published in recent years to tackle these issues by suggesting and investigating the use of various techniques to promote flame stability and enhance combustion efficiency through reactivity-enhancing strategies that reduce reaction time, such as oxygen-enrichment [7–11], preheating [12–14] and catalytic combustion [15–17] or through flow-recirculation-based stabilization mechanisms employing backward facing steps, cavities and bluff bodies as flame holders [8, 18, 19] or a combination of these techniques.

Regarding reactivity-enhancing strategies, Yang et al. [7] carried out numerical simulations to investigate the effect of oxygen-enrichment on the combustion efficiency of lean H2/air flames in a micro-cavity combustor, their results demonstrated that at an O_2 level of 30%, the combustion efficiency could reach up to 98.2% even at high inlet velocity of 32 m/s. Yilmaz et al. [8] employed a combined approach involving the integration of bluff-bodies with different shapes and oxygen-enriched combustion, through CFD simulations. They found that the perforated plate design enhanced heat transfer and fuel efficiency but increased NOx emissions and slightly decreased temperature uniformity. Li et al. [15] numerically demonstrated that oxygen enrichment can significantly enhance both heterogeneous and homogeneous reactions in a non-premixed catalytic micro-combustor leading to dramatic improvement in combustion efficiency. Mansouri [20] conducted a numerical investigation on the effect of wall temperature on premixed CH_4-air flames in a novel wavy micro-channel. The author established that increasing wall temperature causes the flame to move towards the inlet of the micro-combustor, highlighting the sensitivity of flame-location to thermal boundary conditions. Yang et al. [12] examined the impact of inlet mixture temperature on combustion efficiency of ultra-lean H_2/air flame (equivalence ratio $0.3 < \phi < 0.5$) in a cavity-equipped micro-burner. They showed the occurrence of "flame tip opening" phenomenon at $\phi = 0.3$ and $\phi = 0.4$ which leads to fuel leakage and decreases combustion efficiency, but raising inlet temperature mitigated this phenomenon and significantly improved fuel-efficiency. Moreover, Zhang et al. [13] carried out an experimental and numerical study on the effects of preheating and equivalence ratio on combustion characteristics of premixed CH_4/air mixture in three planar micro-channels with different heights. Their findings revealed that preheating not only extended flammability limits but also reduced quenching diameter from 3 to 2 mm, thereby enhancing combustion stability at micro-scale.

As the name implies, flow-recirculation-based stabilization techniques involve the creation of recirculation zones of hot combustion products to form a continuous source of heat and active radicals to ignite incoming reactants and sustain the flame. This is achieved through the incorporation of bluff bodies or cavities that promote localized flow reversal and prolong residence time. Xu et al. [21] and Bagheri et al. [22] addressed numerically the impact of different bluff body shapes on H_2-air flames under various flow conditions. For instance, Xu et al. [21] reported that combustion efficiency increases from 59% to 76% with the increase of bluff body width from 3 to 3.4 mm. Zhang et al. [23] studied the effect of the number of bluff bodies on H_2-air combustion characteristics and concluded that the use of multiple bluff bodies is beneficial for the operation conditions with high inlet velocities. He et al. [24] proposed the use of pin fin array arrangement in H_2-air micro-combustion system. They revealed that the staggered configuration achieved highest external wall heat flux attaining 160 kW/m^2. Gao et al. [25] improved the performance of a traditional cavity micro-burner through the installation of guide vanes. It was shown that this extends flammability limit from 11 to 20 m/s but at the cost of increased pressure losses. Lachraf and Si Ameur [26] proposed new micro combustor design involving on four trapezoidal ribs equidistant distributed on its inner wall. They reported that the ribs generate elongated recirculation zones, which significantly increases the flow residence time. The ribs contributed to increasing the outer wall temperature from 1371.25 to 1417.71 K and promoted a reduced non-uniform temperature zone compared to the backward facing step configuration.

The above review indicates that the micro-combustion based MTPV systems field remains under active investigation, particularly with respect to stable operation under lean conditions. Most existing studies have focused on lean-to-rich equivalence ratios ($0.7 < \phi < 1.4$), where combustion stability is more easily maintained. In contrast, ultra-lean regimes ($\phi < 0.5$) remain insufficiently explored due to the increased susceptibility of the flame to quenching, leaving key aspects of combustor stability, thermal behaviour, and emission characteristics inadequately understood.

The present work builds upon the numerical study of Mansouri et al. [18], who compared the performance of a conventional micro backward-facing step combustor (MBSC) with a novel micro trapped vortex combustor (MTVC). Their results demonstrated that the MTVC design significantly extends the operability range ($0.5 < \phi < 1$), whereas the MBSC was limited to equivalence ratios above 0.7. At $\phi = 0.8$, the MTVC configuration achieved 26.51% higher radiative power, 36% greater radiative efficiency, and 45% lower NOx emissions. Despite these promising results, the performance of the MTVC under ultra-lean conditions remains largely unexplored.

Accordingly, the present study seeks to further optimise the MTVC configuration for operation at an ultra-lean equivalence ratio of $\phi = 0.3$ through a hybrid strategy combining oxygen enrichment with reactant preheating. While oxygen enrichment has been investigated in previous studies [7, 8, 15], these works present notable limitations. Firstly, they typically considered high inlet velocities exceeding 20 m/s, which may lead to significant pressure losses and consequently increased pumping power requirements, potentially reducing the net power output of MTPV systems [27]. Secondly, most investigations were conducted at equivalence ratios close to unity, conditions that may intensify NOx formation and generate substantial thermal stresses on combustor walls due to temperature non-uniformities. Furthermore, to the best of the authors' knowledge, no published studies have examined the combined influence of oxygen enrichment and reactant preheating in

micro-trapped vortex combustors operating under ultra-lean conditions. The integrated strategy proposed in this work therefore aims to enhance the thermal performance and fuel economy of the MTVC configuration while maintaining stable combustion in a highly diluted regime. In doing so, this study provides a comprehensive quantitative assessment of combustor performance in an operating region that has received limited attention in the existing literature.

2 | Numerical Setup

2.1 | Geometric Configuration

The MTVC is visualized in Figure 1. It is a modified version of the conventional MBSC; which includes a bluff-body downstream of the backward-facing step (BFS) called the aft-body (AB) to form a cavity. This design was inspired by aeronautical trapped vortex combustion systems [18]. The combustor size is 10×1.4 mm, with the fluid domain being 10×1 mm. The 2D planar model has been adopted as the aspect ratio of the fluid domain is 10, which falls within the range of 10 to 40 as advised in [28, 29].

2.2 | Mathematical Model

The hypotheses adopted in the present study are as follows. As the calculated maximum Reynolds number of the reacting flow under the investigated conditions (Table 1) doesn't exceed 800, the flow may reasonably be considered laminar. The hydraulic diameter used in the Reynolds number calculation is 0.6 mm, corresponding to the channel height above the aft-body. A steady-state formulation is also adopted. According to the stability diagram of the MTVC reported by Mansouri et al. [18], flow oscillations are expected to occur at velocities of approximately 10 m/s and above at $\phi = 0.3$, whereas the inlet velocity considered in the present study is 7 m/s. Furthermore, the temperatures monitored at different locations within the combustor (e.g., along the centreline and at the outlet) converge to constant values during the simulations, indicating that a steady state is achieved and that no combustion fluctuations occur within the combustor. All surface reactions are disregarded, considering the walls as inert walls. The local thermodynamic properties of the gas mixture are evaluated using the ideal gas law. Air was assumed to consist of only O_2 and N_2.

The mathematical model used to describe the combustion process within the micro-burner incorporates fluid dynamics, heat transfer, and species transport phenomena, and consists of the following set of governing equations:

- Continuity equation:

$$\nabla \bullet (\rho \vec{u}) = 0, \tag{1}$$

where ρ denotes the mass density of the gas mixture and $\vec{u}$ is the velocity field

- Momentum equation:

$$(\vec{u} \bullet \nabla \vec{u}) = -\nabla p + \nabla \bullet \left(\mu \left[\nabla \vec{u} + (\nabla \vec{u})^T - \frac{2}{3} \nabla \bullet \vec{u} \boldsymbol{I} \right] \right), \tag{2}$$

where p is the pressure field, μ is the dynamic viscosity, and $\boldsymbol{I}$ is the unit tensor.

- Energy conservation in the fluid domain:

$$\nabla \bullet \vec{u}(\rho e + p) = \nabla \bullet \left(k_{\text{eff}} \nabla T - \sum_j h_j \vec{J}_j + \mu \left[\nabla \vec{u} + (\nabla \vec{u})^T - \frac{2}{3} \nabla \bullet \vec{u} \boldsymbol{I} \right] \bullet \vec{u} \right) + S_h, \tag{3}$$

where e is the specific total energy, k_{eff} is the effective thermal conductivity of the gas mixture, T is the

TABLE 1 | Boundary conditions.

Inlet	Inlet velocity $U_{\text{in}} = 7$ m/s Equivalence ratio $\phi = 0.3$ Inlet temperature [300–450] K O_2 percentage in air [21–30] %
Outlet	Pressure condition 1 atm
Lower + Upper Outer walls	Mixed convective and radiative heat transfer Convective heat transfer coefficient $h = 10\ \text{W.m}^{-2}.\text{K}^{-1}$ Surface emissivity $\varepsilon = 0.65$ [31] Ambient temperature $T_\infty = 350$ K
Inner walls	No-slip condition Coupled thermal condition Zero-flux condition for all species
Wall material	Stainless steel

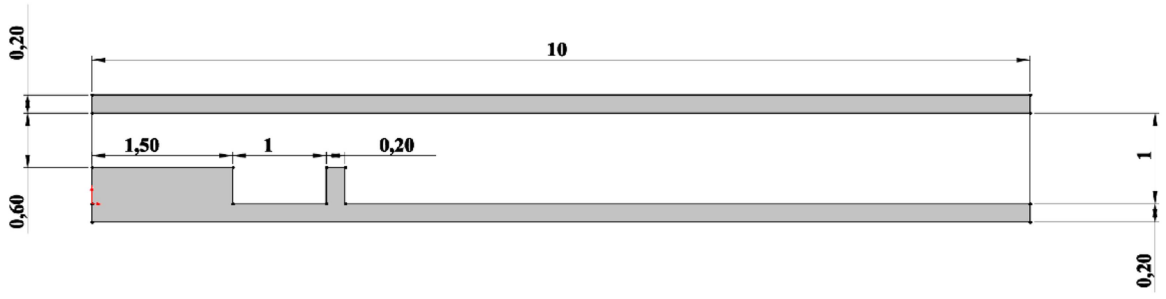

FIGURE 1 | 2D model of the Micro Trapped Vortex Combustor "MTVC" (dimensions in mm).

temperature field, $\vec{J}_j$ and h_j are the diffusion flux and specific enthalpy of species j respectively, S_h is the source term.

- Energy conservation in the solid domain:

$$\nabla\bullet(k_s\bullet\nabla T) = 0, \tag{4}$$

where e is the specific total energy, k_s is the thermal conductivity of the walls.

- Species transport equation:

$$\nabla\bullet(\rho\vec{u}Y_i) = -\nabla\vec{J}_i + R_i, \tag{5}$$

where Y_i and R_i are the mass fraction and the net rate of creation/destruction due to chemical reaction of species i respectively.

The following metrics will be used to quantify the performance of the combustor.

- Radiative power emitted by outer walls:

$$\dot{Q}_{\text{rad}} = \sigma\varepsilon\sum_i A_i\left(T_i^4 - T_\infty^4\right), \tag{6}$$

where ε, σ, T_∞, T_i, A_i are emissivity, Stefan-Boltzmann constant, ambient temperature, temperature and surface area of mesh element i respectively.

- Energy conversion efficiency:

$$\eta_{\text{rad}}(\%) = \frac{\dot{Q}_{\text{rad}}}{\dot{m}_{H_2,\text{in}}\bullet\text{LHV}} \times 100, \tag{7}$$

where $\dot{m}_{H_2,\text{in}}$ is the mass flow rate of H_2 at the inlet, LHV is the lower heating value and is equal to 120 MJ/kg.

- Combustion efficiency:

$$\eta_{\text{comb}}(\%) = \left(1 - \frac{\dot{m}_{H_2,\text{out}}}{\dot{m}_{H_2,\text{in}}}\right) \times 100. \tag{8}$$

- Pollutant concentration at the outlet:

$$[\text{NO}_x](\text{ppb}) = \left(\frac{x_{\text{NO,out}}}{1 - x_{\text{H}_2\text{O,out}}}\right) \times 10^9 \tag{9}$$

where $x_{\text{NO,out}}$ and $x_{\text{H}_2\text{O,out}}$ are the molar fractions of NO and H_2O at the outlet respectively. ppb denotes part per billion per volume. In the evaluation of this metric, only NO species is considered representative of NO_x, whereas NO_2 is neglected under the ultra-lean conditions.

Under lean regime ($\phi < 1$), the complete combustion of hydrogen in air having X_{O_2} mole fraction of oxygen can be represented by the following global equation:

$$\begin{aligned} H_2 + \frac{1}{2\phi X_{O_2}}\left(X_{O_2}O_2 + (1 - X_{O_2})N_2\right) &\rightarrow H_2 \\ O + \frac{1-\phi}{2\phi}O_2 + \frac{1 - X_{O_2}}{2\phi X_{O_2}}N_2 & \end{aligned} \tag{10}$$

It can be readily shown from this equation that the molar fractions of the different species in the hydrogen-air mixture are given by the following expressions:

$$\begin{cases} x_{H_2} = \frac{2\phi X_{O_2}}{2\phi X_{O_2} + 1} \\ x_{O_2} = \frac{X_{O_2}}{2\phi X_{O_2} + 1} \\ x_{N_2} = \frac{1 - X_{O_2}}{2\phi X_{O_2} + 1} \end{cases}. \tag{11}$$

These expressions will be used to specify the molar fractions for each species at the inlet of the combustor.

The simulation of the micro-combustion has been carried out using commercial CFD software ANSYS Fluent. The geometry was discretized using a uniform structured mesh with a cell size of 22 μm which was found to be sufficient to capture the thin structure of the flame as previously reported [18, 20, 30]. Details of the mesh-solution independence study can be found in our work [32]. The coupled pressure-based solver was adopted to handle pressure-velocity coupling. A second order upwind scheme was selected to discretize all of the previously mentioned conservation equations. The P-1 radiation model was selected to deal with internal radiative energy transfers. Gray radiation is used, and the P-1 approach provides a balance between accuracy and computational cost. This choice is supported by our prior comparison with the Discrete Ordinates (DO) model at an inlet temperature of 350 K and an oxygen enrichment of 30%, which showed differences of less than 1.2% in wall temperature and less than 0.9% in maximum flame temperature. H_2/air combustion mechanism with 21 elementary reactions and 10 species was used in the simulations [33] with the stiff chemistry solver to improve stability and convergence of chemical kinetics calculations. The species considered in the mechanism are H_2, O_2, H_2O, OH, H, O, HO_2, H_2O_2, N_2, and Ar. Details of the reaction mechanism and the corresponding elementary reactions can be found in the work of Ó Conaire et al. [33]. NOx formation was modelled using ANSYS Fluent's built-in mechanism, with the thermal and N_2O intermediate pathways activated, while the prompt and fuel NOx pathways were excluded. The prompt pathway is considered negligible in the absence of hydrocarbon radicals, and fuel NOx is irrelevant in hydrogen combustion due to the absence of chemically bound nitrogen in H_2 molecules. The NOx calculations were performed as a post-processing step, representing a decoupled approach. This approach is justified by the very low concentrations of NOx observed in the present study, on the order of parts per billion (Equation 9), indicating that the chemistry of these minor species has a negligible impact on the flow field, temperature distribution, and the concentrations of major combustion products. The convergence criteria were set to 10^{-6} for the energy, radiative transfer and NO_x pollutant equations and 10^{-5} for the rest. In addition, the maximum temperature at the centreline of the combustor, the area-averaged temperature at the outlet as well as the total heat

transfer rate were monitored during iterations. Moreover, a temperature patch of 2000 K has been applied to the entire fluid domain to initiate the combustion reaction. The boundary conditions are summarized in Table 1.

2.3 | Model Validation

The accuracy of the adopted mathematical model and assumptions was validated in our previous work [18], as depicted in Figure 2. Experimental and numerical temperature profiles at the outer walls of a micro-combustor studied by Peng et al. [31], which operates a BFS with an inner step diameter of 1 mm, a combustion section diameter of 3 mm, and a hydrogen-air flame at an equivalence ratio of $\phi = 1$, were compared with the present numerical predictions. Peng et al.'s work involved both experimental measurements and numerical simulations. The results demonstrate that the present CFD model reproduces the experimental wall temperature more accurately than the simulations reported by Peng et al. This validation confirms that the employed numerical approach, including its treatment of flow, heat transfer, and chemical kinetics, is reliable and capable of accurately capturing the thermal behaviour of similar micro-combustion systems.

3 | Results and Discussions

3.1 | Design of Experiments

In the present work, both the inlet temperature of the fresh gas T_{in}, and the oxygen percentage in the air X_{O2} were chosen as input factors influencing the performance of the system, each having four values. For T_{in} the values are 300, 350, 400, and 450 K. The values of X_{O2} are 0.21, 0.24, 0.27 and 0.30. The orthogonal Taguchi design [34] table L16(4^2) is used to organize all 16 cases. The investigated cases along with the corresponding performance parameters are summarized in Table 2. It can be seen that 14 out of 16 cases exhibit stable performance with variation in output parameters depending on oxygen enrichment level and inlet temperature value. However, the remaining two cases when $X_{O2} = 0.3$ and $T_{in} \geq 400$ K marked the onset of the undesirable phenomenon of flame flashback. Under conditions of high inlet temperature and oxygen percentage, the local flame speed exceeds the local flow speed in the cavity, because both preheating and oxygen enrichment boost the reaction rate of combustion, enabling the flame to break free from the cavity where it was meant to be anchored and establish itself at the top of the upstream step. This transition is illustrated in Figure 3, using the OH radical as a key indicator of flame structure.

Flashback is hazardous and can cause severe damage if the flame propagates back to the injectors, thus, these two unstable cases will be excluded from the study and in the next subsections; a more in-depth analysis will be focusing on the 14 stable cases to investigate the effect of inlet conditions on combustor performance.

3.2 | Radiative Power Analysis

The graphs in Figure 4 indicate that radiative power follows a monotonic upward trend as inlet temperature increases from 300 to 450 K across all considered oxygen concentrations. Clearly, oxygen enrichment exerts a stronger effect than preheating based on the vertical spacing between the curves. Specifically, increasing the oxygen concentration from 21% to 30% at constant temperature improves power output by 53.03% and 58.93%, at inlet temperatures of 300 and 350 K, respectively. When the concentration increases from 21% to 27%, the power output rises by 37.16% and 38.7% at inlet temperatures of 400 and 450 K, respectively. Whereas raising inlet temperature from 300 to 450 K at constant oxygen percentage leads to a relatively modest change of 12.67%, 10.92%, and 15.53% at oxygen levels of 21%, 24%, and 27% respectively. This contrast can be explained by the fact that increasing oxygen concentration not only speeds up reaction kinetics, leading to higher rates of chemical energy release but it also weakens the thermal diluting effect of nitrogen [11]. When using atmospheric air as the oxidizer ($X_{O2} = 0.21$), nitrogen which does not participate significantly in the reaction acts as a heat sink, absorbing considerable amount of the released heat, thereby lowering flame and wall temperatures. By replacing this species with the more

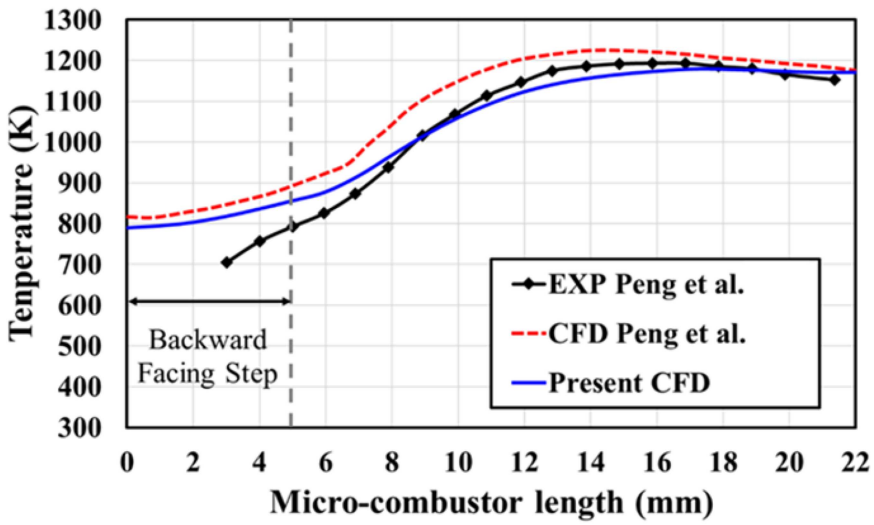

FIGURE 2 | Comparison of the outer wall temperature distribution between simulation results and experimental data.

TABLE 2 | Combustor performance for all simulated cases.

Equivalence ratio $\phi = 0.3$, hydrogen-air mixture flow velocity at the inlet $U_{in} = 7$ m/s					
$T_{\text{in}}(K)$	X_{O_2}	$\dot{Q}_{\text{rad}}(W)$	$[NO_x]$ (ppb)	$\eta_{\text{rad}}(\%)$	$\eta_{\text{comb}}(\%)$
300	0.21	0.459067	0.01540	9.9308	85.6521
	0.24	0.547969	0.19335	10.5363	92.0970
	0.27	0.620913	1.11044	10.7777	96.6791
	0.30	0.702491	4.74023	11.1426	99.0308
350	0.21	0.471462	0.02338	11.9000	94.3850
	0.24	0.549255	0.21481	12.3231	97.4284
	0.27	0.641764	1.32391	12.9986	99.3794
	0.30	0.749339	4.85852	13.8697	99.9230
400	0.21	0.491503	0.03057	14.1795	97.7584
	0.24	0.570693	0.26841	14.6350	99.5561
	0.27	0.674124	1.65772	15.6070	99.9321
	0.30		FLASHBACK		
450	0.21	0.517209	0.04065	16.7876	99.4540
	0.24	0.607818	0,31894	17.5373	99.9248
	0.27	0.717365	1.76225	18.6864	99.9727
	0.30		FLASHBACK		

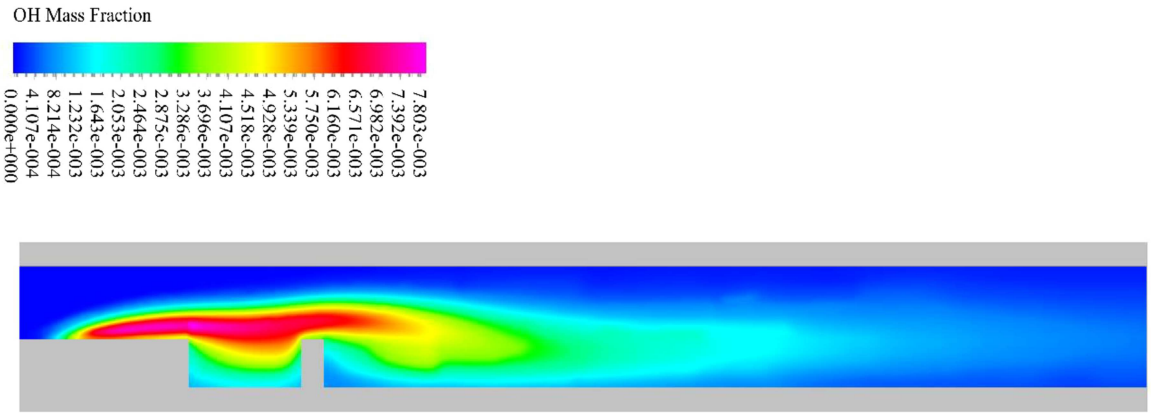

FIGURE 3 | Flame contour showing the occurrence of flashback for the case when $T_{\text{in}} = 400$ K and $X_{O2} = 0.3$.

reactive oxygen, the thermal inertia of the mixture is reduced allowing for more concentrated thermal energy release and elevated local temperatures. This effect is visualized in the outer wall temperature distribution plots in Figure 5 as elevated wall temperatures promote enhanced radiative heat transfer, given that radiative emission scales with the 4th power of temperature. Although preheating increases the flame temperature, it is less effective than oxygen enrichment because the associated decrease in the density of the fresh-gas mixture, which leads to a lower hydrogen mass flow rate (at constant inlet velocity), which in turn reduces the total chemical energy released.

3.3 | Energy Conversion Efficiency Analysis

The assessment of energy conversion efficiency is crucial since it quantifies how much of the total released energy is effectively converted into radiation. Figure 6 shows that radiative efficiency increases with O_2 concentrations across all inlet temperature values. However, in contrast to radiative power, radiative efficiency is primarily influenced by preheating. Increasing the inlet temperature from 300 to 450 K at constant oxygen percentage results in significant enhancement in efficiency by 69.05%, 66.44%, and 73.38% at O2 values of 21%, 24%, and 27% respectively. At $X_{O2} = 0.30$. The maximum inlet temperature is limited to 350 K due flashback, which restricts the attainable improvement in efficiency to 24.48%.

It is known that during combustion, chemical energy is released as heat, a portion of this heat is transferred to the walls of the combustor. This absorbed energy is then emitted through the outer surface of the system due to the transverse temperature gradient between hot reaction products and the cooler ambient environment, or recirculated back to heat the fresh reactive mixture above ignition point driven by the longitudinal temperature gradient between the hot products and cold reactants. When preheated hydrogen-air mixture is introduced, the

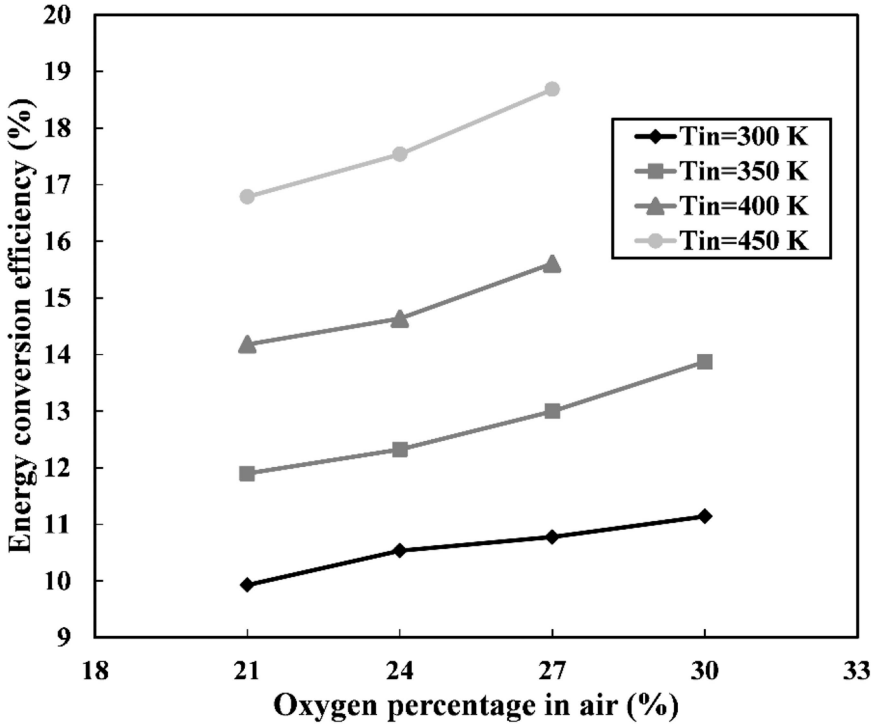

FIGURE 4 | Line plot of radiative power versus inlet temperature at various oxygen enrichment levels.

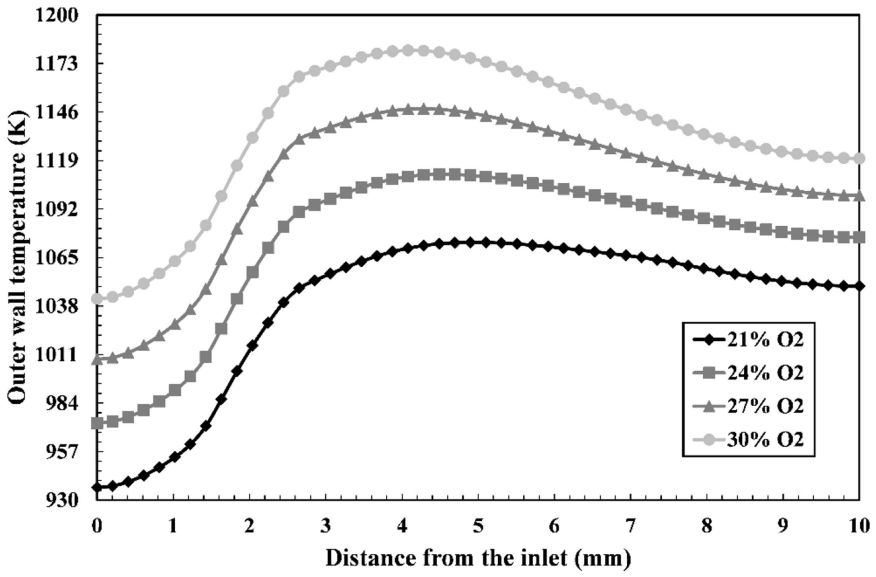

FIGURE 5 | Temperature distribution at the lower outer wall of the combustor at various oxygen enrichments for the case $T_{in} = 350$ K.

longitudinal gradient is reduced, limiting the extent of thermal energy feedback upstream of the flame. This is evidenced in the wall heat flux distribution at the top of the step as indicated in Figure 7. Since the wall heat flux distribution reflects the local thermal energy feedback, its integral over the length of the step corresponds to the amount of heat recirculated into the fresh mixture. From the curves in Figure 7, it is evident that the area under the 450 K profile is smaller compared to the 300 K case, signifying reduced heat recirculation. Hotter reactive mixture requires less energy input to reach ignition temperature, which results in more uniform wall temperature distribution as shown in Figure 8. In particular, the 450 K case exhibits the most uniform outer wall temperature profile, whereas lower inlet temperatures result in larger spatial variations and stronger peaks. Consequently, a greater amount of energy is directed toward the outer surface rather than being internally consumed by the fresh mixture. Additionally, one can notice a gradual shift in the position of the wall hot spot (peak temperature) towards the inlet with each increment in inlet temperature indicating that the flame is approaching the inlet and the mixture preheat zone is reduced. Note that achieving better temperature uniformity at the wall not only significantly promotes energy efficiency, but it is also beneficial to mitigate thermal stresses on the structure of the micro-combustor.

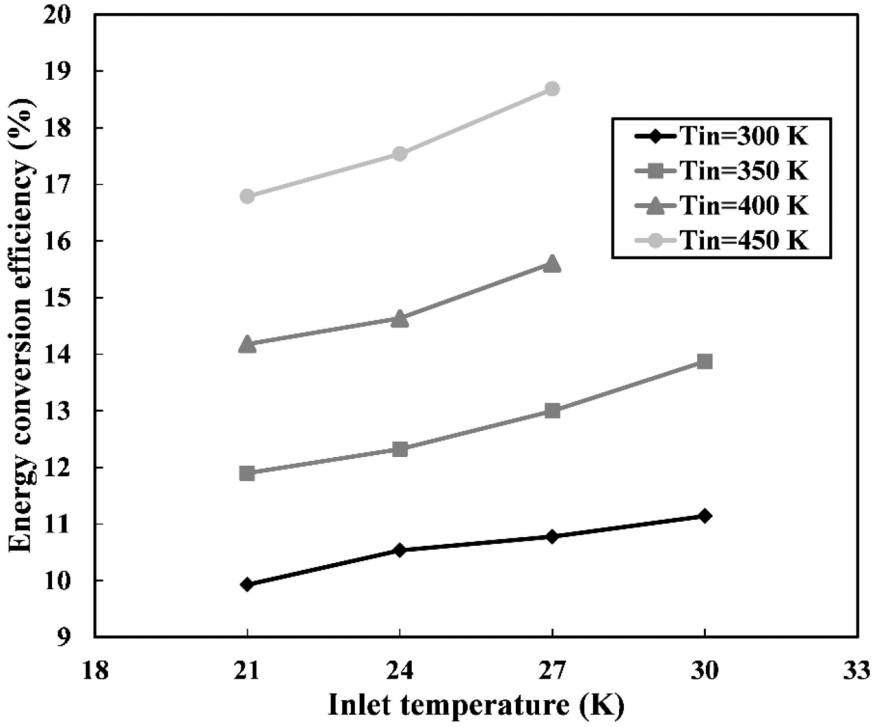

FIGURE 6 | Energy conversion efficiency versus oxygen concentration at different inlet temperatures.

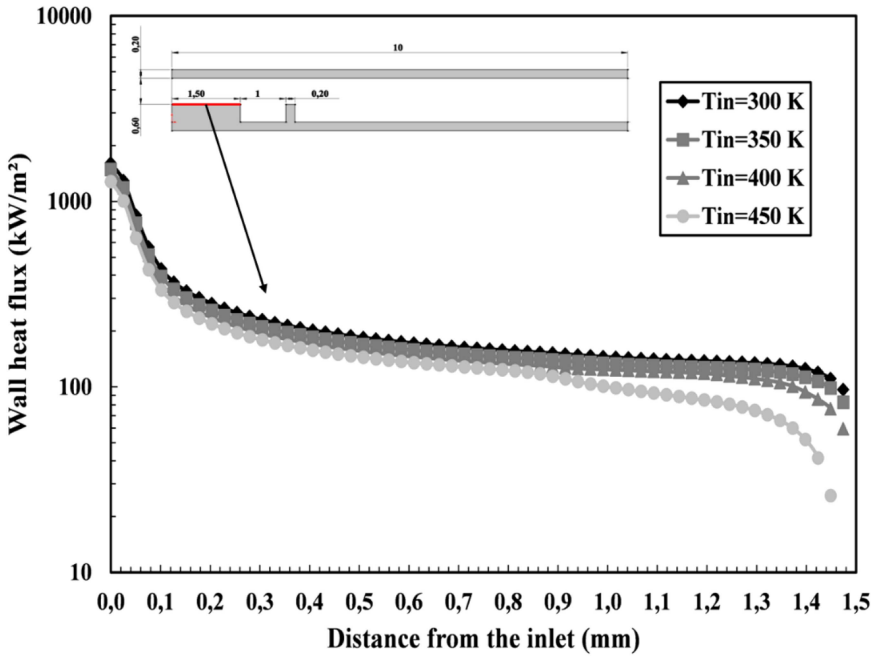

FIGURE 7 | Wall heat flux distribution at the top of the step at various inlet temperatures for $X_{O2} = 0.24$.

3.4 | Combustion Efficiency Analysis

The main effects plots illustrated in Figure 9 show that both studied factors demonstrate a comparable influence on combustion efficiency as inlet temperature raises the efficiency by 6.88% on average while oxygen enrichment by 5.47% on average. This similarity in impact is due to the increase in the rate of combustion reaction induced by the two factors with inlet temperature providing the necessary kinetic energy for reactant molecules to overcome activation energy barrier and combine, thereby amplifying the frequency of molecular collisions, in parallel, oxygen enrichment increases the availability of the oxidizing species (O_2) promoting more complete combustion, the combined effect of these two factors shortens the chemical time scale relative to the residence time of the flow enabling for fuel-efficient combustion.

The effect of oxygen enrichment can be further elucidated by investigating the contours of OH mass fraction represented in Figure 10; clearly, the growing concentration of these reactive

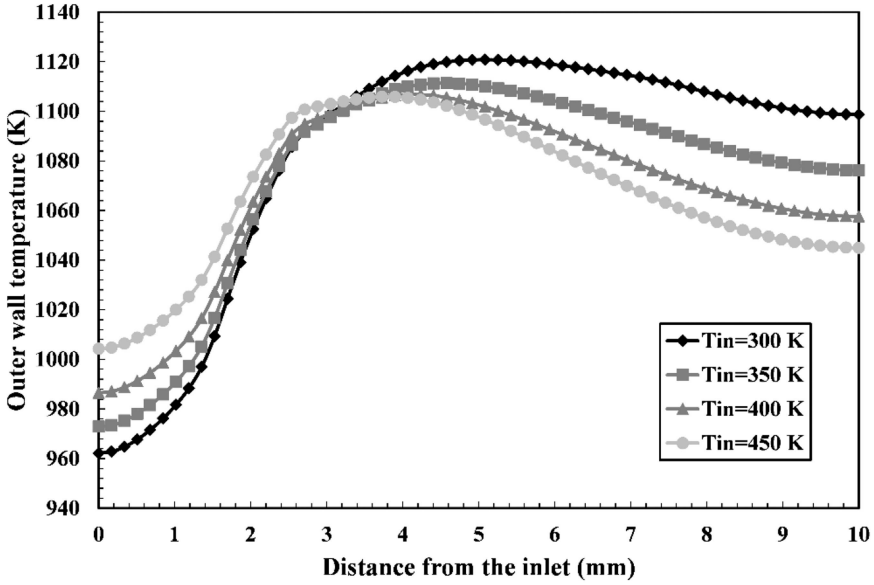

FIGURE 8 | Temperature distribution at the lower outer wall of the combustor at various inlet temperatures for $X_{O2} = 0.24$.

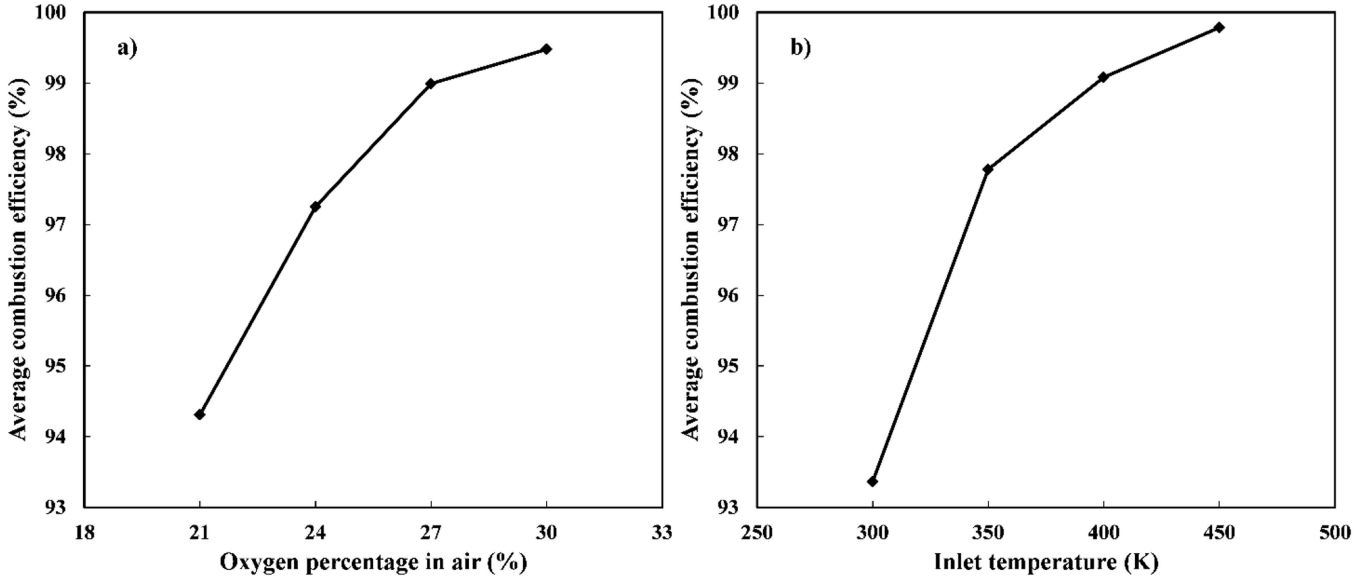

FIGURE 9 | Main effects plots of (a) oxygen enrichment-(b) inlet temperature on combustion efficiency.

intermediates in the cavity region reflects intensified local reaction rates. With higher O_2 levels, OH radicals become more abundant, since O_2 is a key contributor to their formation via the following chain-branching step [35, 36]:

$$H + O_2 \rightarrow OH + O. \quad (12)$$

The rise in OH concentration, in turn, accelerates the consumption of H_2 molecules and therefore enhances combustion efficiency leading to the formation of H_2O [8] through the propagation step:

$$H_2 + OH \rightarrow H + H_2O. \quad (13)$$

Interestingly, this step not only yields the final combustion product (H_2O) but also regenerates H radicals, which feed back into the chain-branching step. This feedback loop sustains OH production and reinforces combustion efficiency under oxygen-enriched conditions.

Complementary evidence about the effect of preheating is provided in Figure 11. At $T_{in} = 300$ K, a portion of hydrogen escapes unburned through the outlet. However, as the inlet temperature increases, the rates of the previously mentioned chain-branching and propagation steps increase according to the Arrhenius equation, promoting earlier radical (O, H, OH) formation, thereby reducing ignition delay. Consequently, the region of unburned hydrogen shifts progressively upstream, indicating earlier fuel consumption. This recession of the fuel-rich zone confirms the acceleration of chemical reactions and earlier flame stabilization under preheated conditions.

This recession in the region of unburned H_2, explains the steeper decline in wall temperature distribution (Figure 8) toward the outlet as T_{in} increases, this behaviour arises because

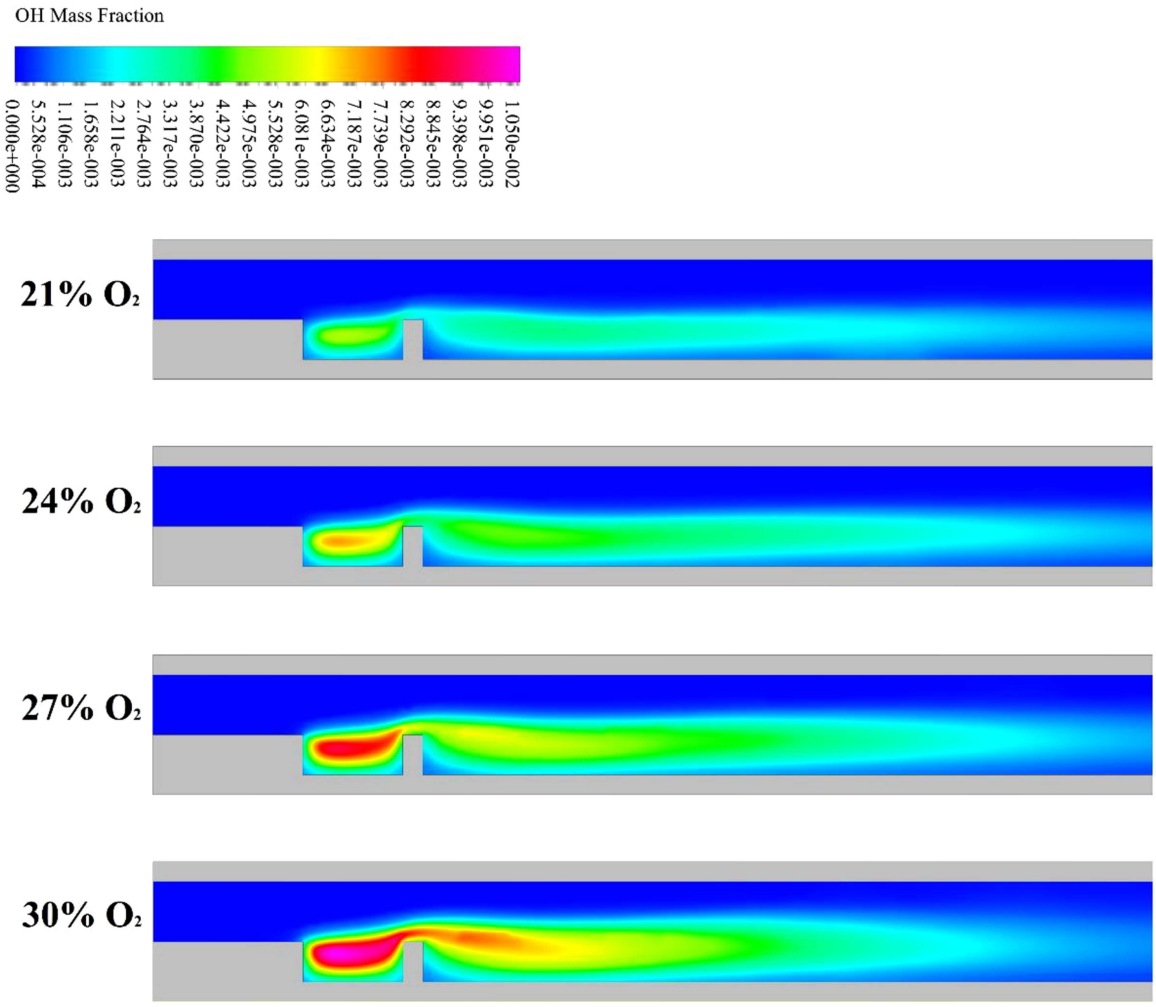

FIGURE 10 | OH contours as flame indicator at different oxygen concentrations for $T_{in} = 350$ K.

preheating shifts the main heat-release region upstream, leaving less unburned fuel to sustain combustion in the downstream section leading to reduced wall heating near the outlet.

3.5 | No_x Emissions Analysis

Despite being a zero-carbon fuel, the burning of hydrogen can still result in the formation of pollutant nitrogen oxides referred to as NO_x due to the high flame temperature, as Figure 12 indicates. Oxygen enrichment causes a serious exacerbation in NO_x emissions at the outlet of the micro-combustor, as increasing O_2 levels in the air at constant inlet temperature amplifies the pollutant emissions at the outlet by a factor of 307.81, 207.81, 54.23 and 43.35 at T_{in} values of 300, 350, 400, and 450 K respectively, while preheating contributes less. As can be inferred from the analysis of radiative power, this high sensitivity to oxygen stems from the high temperature associated with oxygen-rich combustion, for instance, at $T_{in} = 350$ K, increasing X_{O2} from 0.21 to 0.30 raises the flame temperature from 1697.48 to 1945.35 K, amounting to a rise of nearly 250 K, which strongly favours the thermal NO_x formation pathway via the extended Zeldovich mechanism [37].

$$\begin{aligned} &N_2 + O \rightleftharpoons N + NO \\ &k_{1f} = 1.8 \times 10^8 e^{-\frac{38370}{T}}, \end{aligned} \tag{14}$$

$$\begin{aligned} &N + O_2 \rightleftharpoons O + NO \\ &k_{2f} = 1.\,8 \times 10^4 T e^{-\frac{4680}{T}}, \end{aligned} \tag{15}$$

$$\begin{aligned} &N + OH \rightleftharpoons H + NO \\ &k_{3f} = 7.1 \times 10^7 e^{-\frac{450}{T}}, \end{aligned} \tag{16}$$

where k_{1f}, k_{2f} and k_{3f} are the rate constants for the forward reactions expressed in m^3/mol.s.

In addition to being temperature dependent, these reactions show dependency on the concentration of O_2 and OH radicals, as depicted in Figures 10 and 13. NO_x concentrations grow sharply as more oxygen is introduced to the chamber. The contours reveal that at 30% O_2, NO_x levels peak predominantly inside the cavity (reaching a maximum of about 51 ppb) where the flame is anchored and to lesser extent downstream of the aft-body. This zone provides the high thermal and radical-rich environment necessary for the oxidation of nitrogen to NO, consistent with the Zeldovich mechanism and OH contours previously observed in Figure 10. Note that the predicted NO concentrations remain on the order of ppb, the formation of NO_2 (being dependent on NO availability) is expected to be negligible. Therefore, neglecting the contribution of NO_2 to the total NO_x concentration is justified.

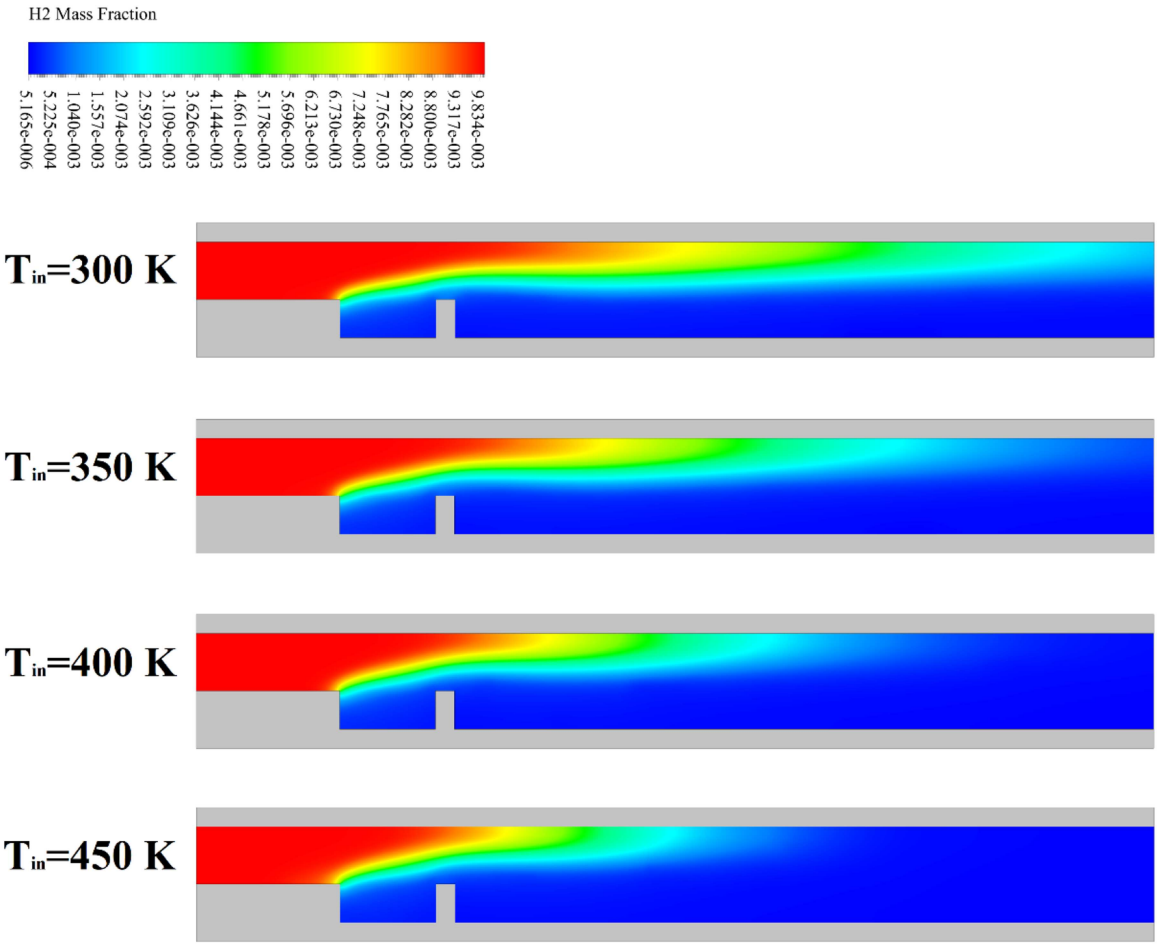

FIGURE 11 | H2 contours at different inlet temperatures for $X_{O2} = 0.24$.

Overall, oxygen enrichment offers clear gains in thermal performance but at the cost of markedly higher NO_x emissions.

3.6 | Performance Comparison With Literature

According to Table 2, the optimal case which offers the most balanced trade-off between radiative power, energy conversion efficiency and pollutant emissions under ultra-lean regime, corresponds to the case for $X_{O2} = 0.27$ and $T_{in} = 450$ K. This case is compared with the lean case at ϕ=0.8 reported by Mansouri et al. [18], as well as with the ultra-lean baseline case using non-preheated atmospheric air (i.e., at $X_{O2} = 0.21$ and $T_{in} = 300$ K). The corresponding performance metrics are summarized in Table 3. The results demonstrate the benefits of oxygen enrichment and preheating in boosting the thermal performance of the micro-combustor under ultra-lean regime. Compared with the lean case ($\phi = 0.8$), it can be noticed that although the MTVC can operate at an ultra-lean regime $\phi = 0.3$, it suffers a severe degradation in thermal performance, as its power output is lower by 47.54%, while the radiation efficiency drops from 13.25% to 9.93%, while almost no trace of NO_x are emitted. Whereas the present proposed optimal case ($\phi = 0.3$ with higher oxygen and inlet temperature) demonstrates better thermal performance by limiting the loss in power to only 18%. This trade-off is tolerable given the substantial 62.5% decrease in equivalence ratio. Moreover, energy efficiency is remarkably improved, even outperforming the lean case at $\phi = 0.8$. Notably,

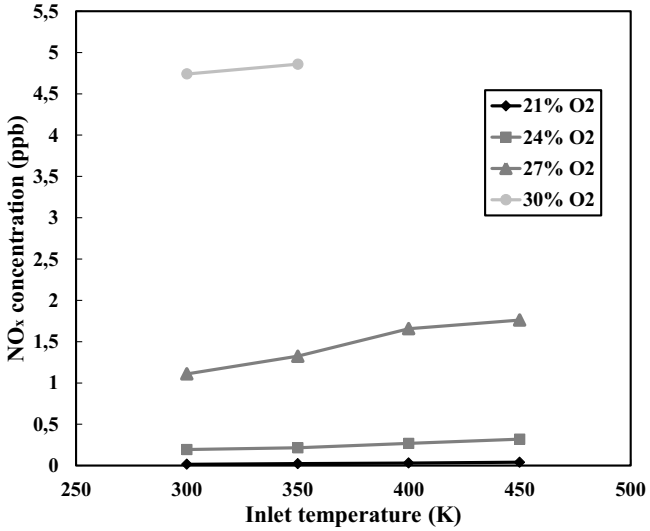

FIGURE 12 | NO_x emissions at the outlet versus inlet temperature at various oxygen enrichment levels.

NO_x emissions in the optimal configuration are 99.12% lower than those at $\phi = 0.8$, despite the use of preheated oxygen-enriched air.

These results show that preheating and oxygen enrichment are highly effective at augmenting the thermal performance of

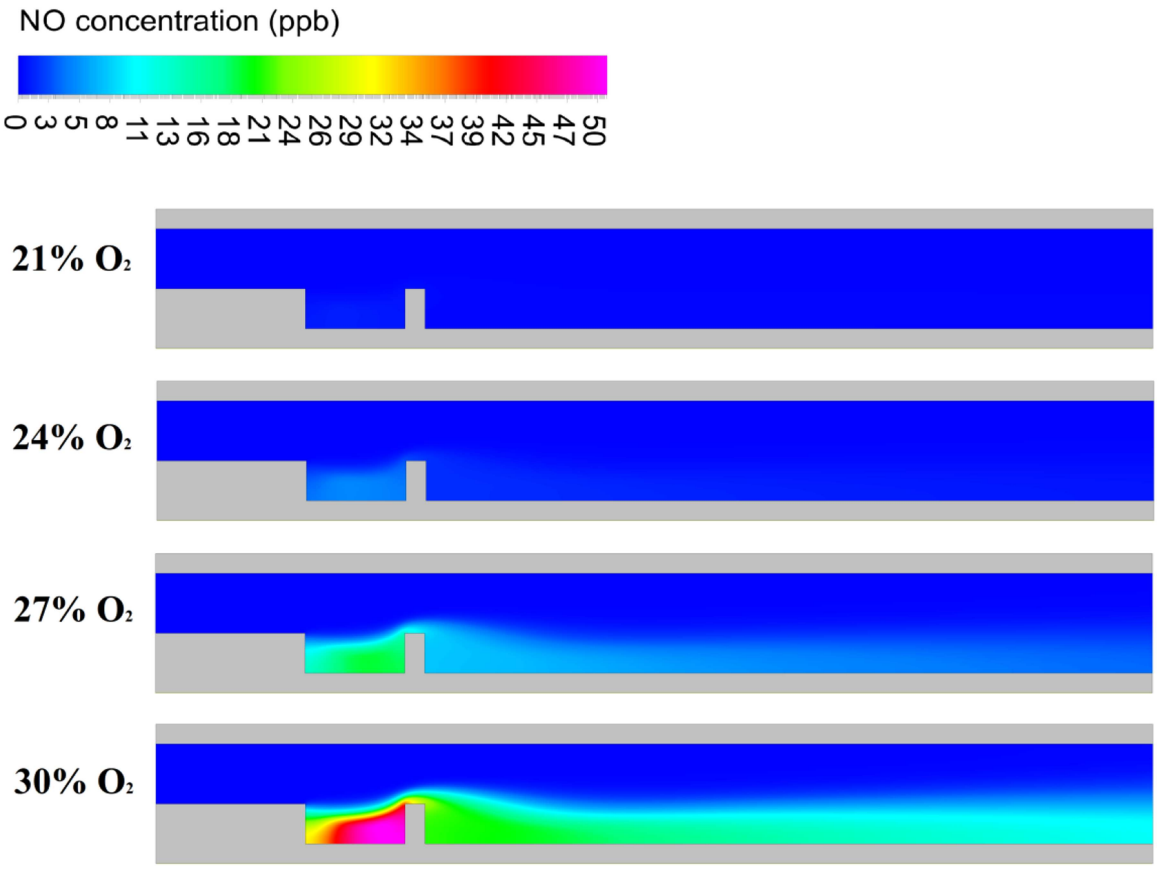

FIGURE 13 | NO_x concentration contours at $T_{in} = 350$ K.

TABLE 3 | Comparison between the case of Mansouri et al and the present study.

	Mansouri et al. [18]	Current work	
Equivalence ratio ϕ	0.8	0.3	0.3
Flow velocity at the inlet U_{in} (m/s)	7	7	7
Inlet temperature T_{in} (K)	300	300	450
O_2(%) in air	21	21	27
Radiative power Q_{rad} (W)	0.875	0,459	0.717
Energy efficiency η_{rad} (%)	13.25	9.93	18.69
NOx emissions at the outlet (ppbv)	~200	0.05	1.77

MTPV systems under ultra-lean regime, thereby enabling fuel-efficient performance across a broader range of equivalence ratios.

4 | Conclusion

A parametric numerical investigation was conducted to evaluate how preheating and oxygen enrichment significantly improve the thermal performance, without comprising flame stability and NOx emissions, of a novel hydrogen-powered micro-trapped vortex combustor operating at an ultra-lean equivalence ratio ($\phi = 0.3$).

The findings showed that excessive O_2 enrichment at 30% combined with high inlet temperature $T_{in} = 450$ K leads to flame flashback pointing out a safety threshold. This study concludes the following. Performance analysis within the stable operating region showed that both factors affect performance parameters with varying degrees of influence. O_2 enrichment strongly boosted radiative power output through higher wall temperatures and reduced thermal dilution at the cost of increased NO_x emissions. As for preheating, it was shown to be effective in enhancing the energy conversion efficiency of the system, by mitigating wall temperature gradients. Regarding combustion efficiency, both factors (oxygen enrichment and mixture preheating) exhibited nearly equal impacts. The optimal case is when both T_{in} and X_{O2} are at 450 K and 0.27 respectively, which offered a strong compromise between thermal performance and emissions. This has led to an improvement of 56.20% in terms of radiative power and 88.22% in terms of energy efficiency over the unheated air

baseline ($T_{in} = 300$ K and $X_{O2} = 0.21$) with NO_x still low. When compared to the lean case at $\phi = 0.8$ from literature, the present ultra-lean optimal case sacrificed about 18% of power output, yet delivered 41% higher radiative efficiency and 99% lower pollutant emissions.

Author Contributions

Anouar Benzitouni: data curation, formal analysis, investigation, visualization, writing – original draft. **Abdelhakim Settar:** methodology, resources, software, supervision, writing – review and editing. **Boudinar Naouam:** funding acquisition, project administration, resources, supervision, writing – review and editing). **Salaheddine Azzouz:** conceptualization, funding acquisition, project administration, supervision, writing – review and editing. **Zakaria Mansouri:** conceptualization, methodology, resources, software, supervision, validation, writing – review and editing.

Acknowledgments

This work was supported by the Algerian Ministry of Higher Education and Scientific Research.

Conflicts of Interest

The authors declare no conflicts of interest.

Declaration of Generative AI in the Writing Process

During the preparation of this work the first author used Chat GPT in order to polish the language of some sections of the paper and improve readability. After using this tool, all authors reviewed and edited the content as needed and take full responsibility for the content of the publication.

Data Availability Statement

The data that support the findings of this study are available from the corresponding author upon reasonable request.

References

1. A. D. Stazio, "Experimental Characterization of the Combustion Dynamics at Micro-Scale Caractérisation expérimentale de la dynamique de la combustion à micro-échelle," (PhD Thesis Université d'Orléans, 2016), https://theses.hal.science/tel-01994718v1.

2. M. Nauman, J. Pan, Y. Wang, F. Li, A. Oluwaleke Ojo, and A. Raza, "A Review of Recent Advancements in Micro Combustion Techniques to Enhance Flame Stability and Fuel Residence Time," *International Journal of Hydrogen Energy* 49 (2024): 1165–1193.

3. A. Datas and R. Vaillon, "Thermophotovoltaic Energy Conversion," in Ultra-High Temperature Thermal Energy Storage, Transfer and Conversion, ed: Woodhead Publishing - Elsevier (2020).

4. Y. Yan, Z. He, Q. Xu, et al., "Numerical Study on Premixed Hydrogen/Air Combustion Characteristics in Micro–Combustor With Slits on Both Sides of the Bluff Body," *International Journal of Hydrogen Energy* 44 (2019): 1998–2012.

5. L. Guo, M. Zhai, S. Xu, Q. Shen, P. Dong, and X.-S. Bai, "Flame Characteristics of Methane/Air With Hydrogen Addition in the Micro Confined Combustion Space," *International Journal of Hydrogen Energy* 47 (2022): 19319–19337.

6. J. E., Y. Mei, C. Feng, J. Ding, L. Cai, and B. Luo, "A Review of Enhancing Micro Combustion to Improve Energy Conversion Performance in Micro Power System," *International Journal of Hydrogen Energy* 47 (2022): 22574–22601.

7. W. Yang, L. Li, A. Fan, and H. Yao, "Effect of Oxygen Enrichment on Combustion Efficiency of Lean H2/N2/O2 Flames in a Micro Cavity-Combustor," *Chemical Engineering and Processing-Process Intensification* 127 (2018): 50–57.

8. H. Yilmaz, "Investigation of Combustion and Emission Performance of a Micro Combustor: Effects of Bluff Body Insertion and Oxygen Enriched Combustion Conditions," *International Journal of Hydrogen Energy* 44 (2019): 25985–25999.

9. D. Wang, C. Ji, S. Wang, Z. Wang, J. Yang, and Q. Zhao, "Numerical Study on the Premixed Oxygen-Enriched Ammonia Combustion," *Energy & Fuels* 34 (2020): 16903–16917.

10. N. Merlo, T. Boushaki, C. Chauveau, et al., "Experimental Study of Oxygen Enrichment Effects on Turbulent Non-Premixed Swirling Flames," *Energy & Fuels* 27 (2013): 6191–6197.

11. H. A. Alabaş and B. Albayrak Çeper, "Effect of Oxygen Enrichment on the Combustion Characteristic and Pollutant Emissions of Kerosene-Biogas Mixtures on a Mini Jet Engine Combustion Chamber," *Journal of the Energy Institute* 111 (2023/12/01/2023): 101420.

12. W. Yang, A. Fan, and H. Yao, "Effect of Inlet Temperature on Combustion Efficiency of Lean H2/air Mixtures in a Micro-Combustor With Wall Cavities," *Applied Thermal Engineering* 107 (2016): 837–843.

13. Y. Zhang, J. Pan, A. Tang, Q. Lu, Z. Zha, and S. Bani, "Effects of Inlet Parameters on Combustion Characteristics of Premixed CH4/Air in Micro Channels," *Journal of the Energy Institute* 92 (2019): 824–834.

14. L. Ma, Q. Fang, C. Zhang, and G. Chen, "A Novel Swiss-Roll Micro-Combustor With Double Combustion Chambers: A Numerical Investigation on Effect of Solid Material on Premixed CH4/air Flame Blow-Off Limit," *International Journal of Hydrogen Energy* 46 (2021): 16116–16126.

15. L. Li, S. Wang, L. Zhao, and A. Fan, "A Numerical Investigation on Non-Premixed Catalytic Combustion of CH4/(O2 + N2) in a Planar Micro-Combustor," *Fuel* 255 (2019): 115823.

16. Y. Zhang, J. Pan, Y. Zhu, et al., "The Effect of Embedded High Thermal Conductivity Material on Combustion Performance of Catalytic Micro Combustor," *Energy Conversion and Management* 174 (2018): 730–738.

17. L. Li, G. Yang, and A. Fan, "Non-Premixed Combustion Characteristics and Thermal Performance of a Catalytic Combustor for Micro-Thermophotovoltaic Systems," *Energy* 214 (2021): 118893.

18. Z. Mansouri, L. Chouichi, S. Azzouz, and A. Settar, "A Novel Micro-Thermophotovoltaic Combustor of Hydrogen–Air to Enable Ultra-Lean Combustion, High Thermal Output and NO Low Emissions," *International Journal of Energy Research* 2025 (2025): 4352411.

19. J. Wan, Y. Wu, and H. Zhao, "Excess Enthalpy Combustion of Methane-Air in a Novel Micro Non-Premixed Combustor With a Flame Holder and Preheating Channels," *Fuel* 271 (2020): 117518.

20. Z. Mansouri, "Combustion in Wavy Micro-Channels for Thermo-Photovoltaic Applications – Part I: Effects of Wavy Wall Geometry, Wall Temperature Profile and Reaction Mechanism," *Energy Conversion and Management* 198 (2019): 111155.

21. F. Xu, Y. Yan, Z. He, Z. Yang, and L. Zhang, "Numerical Study on the Influence of Controllable Flow Ratio on Combustion Characteristics of a Controllable Central Slotted Bluff Body and Cavity Combined Micro Combustor," *International Journal of Hydrogen Energy* 46 (2021): 6901–6914.

22. G. Bagheri, S. E. Hosseini, and M. A. Wahid, "Effects of Bluff Body Shape on the Flame Stability in Premixed Micro-Combustion of Hydrogen–Air Mixture," *Applied Thermal Engineering* 67 (2014): 266–272.

23. Y. Zhang, Q. Lu, B. Fan, L. Long, E. K. Quaye, and J. Pan, "Effect of Multiple Bluff Bodies on Hydrogen/Air Combustion Characteristics and

Thermal Properties in Micro Combustor," *International Journal of Hydrogen Energy* 48 (2023): 4064–4072.

24. Z. He, Y. Yan, F. Xu, et al., "Combustion Characteristics and Thermal Enhancement of Premixed Hydrogen/Air in Micro Combustor With Pin Fin Arrays," *International Journal of Hydrogen Energy* 45 (2020): 5014–5027.

25. W. Gao, Y. Yan, K. Shen, L. Huang, T. Zhao, and B. Gao, "Combustion Characteristic of Premixed H2/air in the Micro Cavity Combustor With Guide Vanes," *Energy* 239 (2022): 121975.

26. A. Lachraf and M. Si Ameur, "Numerical Investigation of Thermal Performance of Hydrogen Fueled Micro-Combustor With Trapezoidal Ribs," *International Journal of Hydrogen Energy* 48 (2023): 39570–39585.

27. M. Wang, P. Li, and F. Wang, "Dependence of the Blowout Limit on Flow Structure, Heat Transfer, and Pressure Loss in a Bluff-Body Micro-Combustor," *International Journal of Hydrogen Energy* 45 (2020): 19912–19925.

28. Y. Zhang, Q. Lu, B. Fan, et al., "Effect of Intake Method on Ammonia/Oxygen Non-Premixed Combustion in the Micro Combustor With Dual-Inlet," *Fuel* 317 (2022): 123504.

29. Y. Zhang, S. Xiao, Q. Lu, W. Chen, E. K. Quaye, and J. Pan, "Numerical Study on Non-Premixed Combustion Characteristics of NH3/O2 in Multi-Inlet Micro Combustor," *Applied Thermal Engineering* 224 (2023): 120091.

30. Z. Mansouri, "A Novel Wavy Micro-Combustor for Micro-Thermophotovoltaic Applications," *Chemical Engineering and Processing - Process Intensification* 163 (2021): 108371.

31. Q. Peng, Y. Wu, J. E, W. Yang, H. Xu, and Z. Li, "Combustion Characteristics and Thermal Performance of Premixed Hydrogen-Air in a Two-Rearward-Step Micro Tube," *Applied Energy* 242 (2019): 424–438.

32. L. Chouichi, S. Azzouz, Z. Mansouri, M. Said, A. Settar, and M. Kahaleras, "Combustion Science and Technology Objective Optimization of a Novel Micro Trapped Vortex Combustor for Thermophotovoltaic Systems Using CFD and RSM Objective Optimization of a Novel Micro Trapped Vortex Combustor for Thermophotovoltaic Systems Using CFD and RSM," *Combustion Science and Technology* (2025): 1–32, https://doi.org/10.1080/00102202.2025.2598441.

33. M. Ó Conaire, H. J. Curran, J. M. Simmie, W. J. Pitz, and C. K. Westbrook, "A Comprehensive Modeling Study of Hydrogen Oxidation," *International Journal of Chemical Kinetics* 36 (2004): 603–622.

34. J. M. Cimbala, "Taguchi Orthogonal Arrays," ed. Pennsylvania State University (2014), pp. 1–3.

35. C. K. Law, Combustion Physics. Cambridge: Cambridge University Press (2006).

36. T. Engel and P. Reid, Physical Chemistry: Thermodynamics, Statistical Thermodynamics, and Kinetics, 4th ed. New York: Pearson (2018).

37. Y. B. Zeldovich and R. A. Sunyaev, "25. The Oxidation of Nitrogen in Combustion and Explosions," (1992).